Swart, P.K., Eberli, G.P., Malone, M.J., and Sarg, J.F. (Eds.), 2000
Proceedings of the Ocean Drilling Program, Scientific Results, Vol. 166

9. MINOR AND TRACE ELEMENTS IN INTERSTITIAL WATERS OF THE GREAT BAHAMA BANK: RESULTS FROM ODP LEG 166[1]

Eric Heinen De Carlo[2] and Philip A. Kramer[3]

ABSTRACT

Concentrations of minor and trace elements (Li, Rb, Sr, Ba, Fe, and Mn) in interstitial water (IW) were found in samples collected during Ocean Drilling Program (ODP) Leg 166 from Sites 1005, 1006, and 1007 on the western flank of the Great Bahama Bank (GBB). Concentrations of Li range from near-seawater values immediately below the sediment/water interface to a maximum of 250 µM deep in Site 1007. Concentrations determined during shore-based studies are substantially lower than the shipboard data presented in the Leg 166 *Initial Reports* volume (range of 28–439 µM) because of broad-band interferences from high dissolved Sr concentrations in the shipboard analyses. Rubidium concentrations of 1.3–1.7 µM were measured in IW from Site 1006 when salinity was less than 40 psu. A maximum of 2.5 µM is reached downhole at a salinity of 50 psu. Shipboard and shore-based concentrations of Sr^{2+} are in excellent agreement and vary from 0.15 mM near the sediment water interface to 6.8 mM at depth. The latter represent the highest dissolved Sr^{2+} concentrations observed to date in sediments cored during the Deep Sea Drilling Project (DSDP) or ODP. Concentrations of Ba^{2+} span three orders of magnitude (0.1–227µM). Concentrations of Fe (<0.1–14 µM) and Mn (0.1–2 µM) exhibit substantially greater fluctuations than other constituents.

The concentrations of minor and trace metals in pore fluids from the GBB transect sites are mediated principally by changes in pore-water properties resulting from early diagenesis of carbonates associated with microbial degradation of organic matter, and by the abundance of detrital materials that serve as a source of these elements. Downcore variations in the abundance of detrital matter reflect differences in carbonate production during various sea-level stands and are more evident at the more proximal Site 1005 than at the more pelagic Site 1006. The more continuous delivery of detrital matter deep in Site 1007 and throughout all of Site 1006 is reflected in a greater propensity to provide trace elements to solution.

Concentrations of dissolved Li^{+} derive principally from (1) release during dissolution of biogenic carbonates and subsequent exclusion during recrystallization and (2) release from partial dissolution of Li-bearing detrital phases, especially ion-exchange reactions with clay minerals. A third but potentially less important source of Li^{+} is a high-salinity brine hypothesized to exist in Jurassic age (unsampled) sediments underlying those sampled during Leg 166. The source of dissolved Sr^{2+} is almost exclusively biogenic carbonate, particularly aragonite. Concentrations of dissolved Sr^{2+} and Ba^{2+} are mediated by the solubility of their sulfates. Barite and detrital minerals appear to be the more important source of dissolved Ba^{2+}. Concentrations of Fe and Mn^{2+} in anoxic pore fluids are mediated by the relative insolubility of pyrite and incorporation into diagenetic carbonates. The principal sources of these elements are easily reduced Fe-Mn-rich phases including Fe-rich clays found in lateritic soils and aoelian dust.

INTRODUCTION

A series of holes was drilled on the western flank of the Great Bahama Bank (GBB) during Ocean Drilling Program (ODP) Leg 166. Of these, Sites 1003–1007, which are located in the Straits of Florida at the north end of the Santaren Channel (Fig. 1), comprise a transect from shallow to deep water that drilled through late Oligocene- to Holocene-age prograding carbonate sequences (Fig. 2). A major objective of Leg 166 was to investigate the significance of fluid flow through the margin of the GBB. This objective was met by a combination of in situ temperature measurements and a high-resolution interstitial water (IW) sampling program. Recovered fluids were exhaustively analyzed for a variety of major, minor, and trace constituents (Eberli, Swart, Malone, et al., 1997). Two other holes, Clino and Unda, which were drilled in 7 m of water during the Bahamas Drilling Project (1990), provided data from proximal sites on the western margin of the GBB that complement data collected during ODP Leg 166 and the subsequent postcruise research (Eberli, Swart, Malone, et al., 1997).

Water/rock interactions and large-scale fluid circulation within sedimentary deposits on continental margins represent the most important chemical transport mechanisms within margins. These processes contribute to the transfer of elements from the lithosphere to the hydrosphere and to global biogeochemical cycles. Microbial activity and inorganic chemical reactions within the sediments control the diagenesis of sediments and the concomitant alteration of fluid chemistry. Fluid flow enhances microbial activity deep in the sedimentary column and acts as a conveyor belt that imports a stream of reactants and exports the end products of organic matter degradation. Interactions between water, rock, and organic matter also alter rock porosity and permeability. Thus, diagenetic processes alter not only the chemical and physical properties of the sediments, but because fluid flow is frequently concentrated along distinct intervals within the sediments, the affected sedimentary sequences can often be converted into lithified horizons that define seismic sequence boundaries.

In this paper we present results of shore-based minor and trace element analyses of interstitial waters collected from Sites 1005, 1006, and 1007. Elements reported include Li, Rb, Sr, Ba, Fe, and Mn. The results of Fe, Li, and Sr analyses are compared to preliminary data generated aboard *JOIDES Resolution* during Leg 166, and are discussed in terms of constraints inherent in the analytical methods used to determine their concentrations. The concentrations of dissolved Li, Rb, Ba, Fe, and Mn reported herein are also discussed in terms of their geochemical significance, in particular their relationship to diagenetic reactions resulting from the oxidation of organic matter in a carbonate dominated environment.

[1]Swart, P.K., Eberli, G.P., Malone, M.J., and Sarg, J.F. (Eds.), 2000. *Proc. ODP, Sci. Results,* 166: College Station TX (Ocean Drilling Program).

[2]Department of Oceanography, School of Ocean and Earth Science and Technology, 1000 Pope Road, University of Hawaii at Manoa, Honolulu HI 96822, USA. edecarlo@soest.hawaii.edu.

[3]Department of Marine Geology and Geophysics, Rosenstiel School of Marine and Atmospheric Science, University of Miami, 4600 Rickenbacker Causeway, Miami FL 33149, USA.

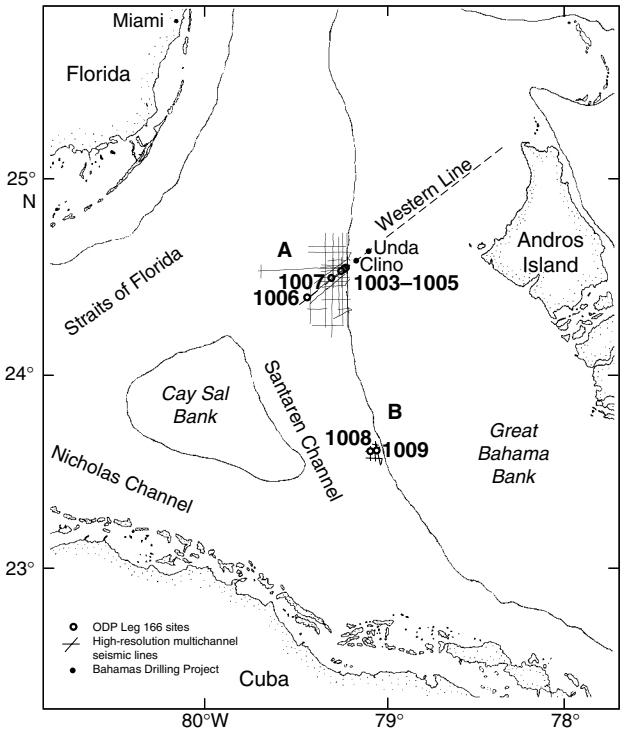

Figure 1. Location map of the Bahamas showing Leg 166 site-survey lines. Sites 1003 through 1007 are located in area A. Sites 1008 and 1009 are located in area B (from Shipboard Scientific Party, 1997a).

Regional Geology

The Bahamas Archipelago consists of a series of isolated carbonate platforms located on the southern tip of the eastern continental margin of North America. This margin has its beginning in the Jurassic period during the opening of the Atlantic Ocean. The southern portion of the margin collided with the Caribbean plate in the Late Cretaceous, reaching the greatest intensity in the Eocene (Ball et al., 1985; Walles, 1993; Denny et al., 1994). Upon a shift of the plate boundary to south of the island of Cuba at the end of the Eocene, tectonic activity subsided and Cuba remained attached to the southern portion of the American continental margin.

Significant debate continues regarding the foundation of the Bahamas platform. Two questions central to this debate are: (1) Is the Bahamian basement of continental or oceanic origin? and (2) Is the horst and graben topography that formed during the Jurassic rift stage still reflected in the modern platform pattern (Mullins and Lynts, 1977; Sheridan et al., 1981)? The seismic refraction evidence available to date does not allow unequivocal identification of the basement as being either continental or oceanic crust. Thus, drilling of the Bahamas platform margin was considered key to resolving the controversy between the horst and graben and megabank hypotheses.

Fluid flow or recharge in the GBB is evidenced from the nonsteady-state profiles of conservative and nonconservative species in the IW recovered from the uppermost 100 m of the sediments at Sites 1003–1007 (Eberli, Swart, Malone, et al., 1997). A "flushed zone" was identified to occur within the top 30–50 meters below seafloor (mbsf) through a general lack of geochemical gradients, with most IW constituents displaying concentrations near those of bottom seawater. Progressing seaward, the flushed zone decreases in thickness; and in the case of Sites 1006 and 1007, a small but significant gradient in the concentration of Sr is observed in pore water from this zone. It was, therefore, inferred that more subdued flushing occurs within a thinner zone (~25–30 m) at the two more distal sites relative to the GBB proximal sites. Below the flushed zone at each of the transect sites, sharp variations occur in concentrations of IW constituents. Gradients of nonconservative elements are nonsteady-state and reflect the occurrence of downward advecting fluids as well as local reaction zones. Large increases in Cl^- concentrations occur at all sites as a function of depth and suggest the existence of a deep-seated high-salinity brine or evaporite deposits. Even within the predominantly conservative profiles of species such as Cl^-, small perturbations in concentrations that cannot be attributed to analytical error are observed. These appear to correlate with changes in physical properties of the corresponding sediments and may reflect horizontal fluid migration along sequence boundaries.

METHODS

Interstitial Water Recovery and Handling

Methods for recovery of IW and details of the sample handling are described in Eberli, Swart, Malone, et al. (1997). All IW samples were double filtered. Samples were initially collected from the squeezer through 0.45-µm Gelman polysulfone disposable filters and into scrupulously cleaned 50-mL plastic syringes. The IW was subsequently refiltered through either 0.45-µm Gelman polysulfone disposable filters or acid-washed 0.2-µm Gelman polysulfone disposable filters. The latter was performed when collecting IW samples for shore-based trace element analyses. Trace element samples were stored in acid-washed plastic bottles, acidified with 50 µL of ultra-high purity HNO_3, sealed with parafilm and chilled until analysis.

Analytical Methods

Shore-based analyses of IW constituents were performed by atomic spectrometry and flow injection analysis (FIA). Dissolved Li^+ and Rb^+ were determined by atomic emission spectrometry (AES) using the method of standard additions on a Perkin-Elmer Model 603 double beam spectrometer. Lithium determinations were carried out at 670.8 nm using a slit width of 0.2 nm. The atomic emission of Rb was measured at 780 nm also using a 0.2 nm slit width. Because IW can show wide variations in matrix composition (e.g., salt concentrations), a background correction technique developed in our laboratory for analysis of geothermal and hydrothermal fluids was used (C. Fraley and E. De Carlo, unpubl. data). This method compensates for the large background absorption signals such as those encountered in high salinity recovered deep within the Bahamas Transect sites (Eberli, Swart, Malone, et al., 1997). Our offline background correction technique involves measurement of the emission intensity of the solution at the analytical wavelength, then measuring the emission signal 0.8 nm above and below the analytical line of the element of interest. Because atomic emission lines are very narrow (e.g., Robinson, 1990), the online measurement yields the emission intensity derived from the analyte and the matrix background, whereas the offline signal originates only from the matrix. Matrix absorption is typically of a broad-band nature, thus subtraction of the linearly interpolated background signal obtained during the two offline measurements from the online emission measurement yields a reliable analyte signal.

Dissolved Ba^{2+} and Sr^{2+} were determined by inductively coupled plasma-optical emission spectroscopy (ICP/OES) using a high-resolution Leeman Labs model PS1 echelle grating spectrometer (e.g., De Carlo, 1992). Instruments were calibrated using a series of dilutions of IAPSO seawater (Sr^{2+}), or by preparation of single-element standards (Ba^{2+}) in a NaCl matrix.

Dissolved Fe^{2+} and Mn^{2+} were determined by FIA with fluorescence detection (Resing and Mottl, 1992) and/or by ICP/OES. Standards for Fe and Mn analysis were prepared by spiking acidified surface seawater with appropriate amounts of certified single-element spectroscopic standards. IW samples were diluted with oligotrophic surface seawater as necessary to ensure that instrumental signals fell within the linear portion of the calibrations.

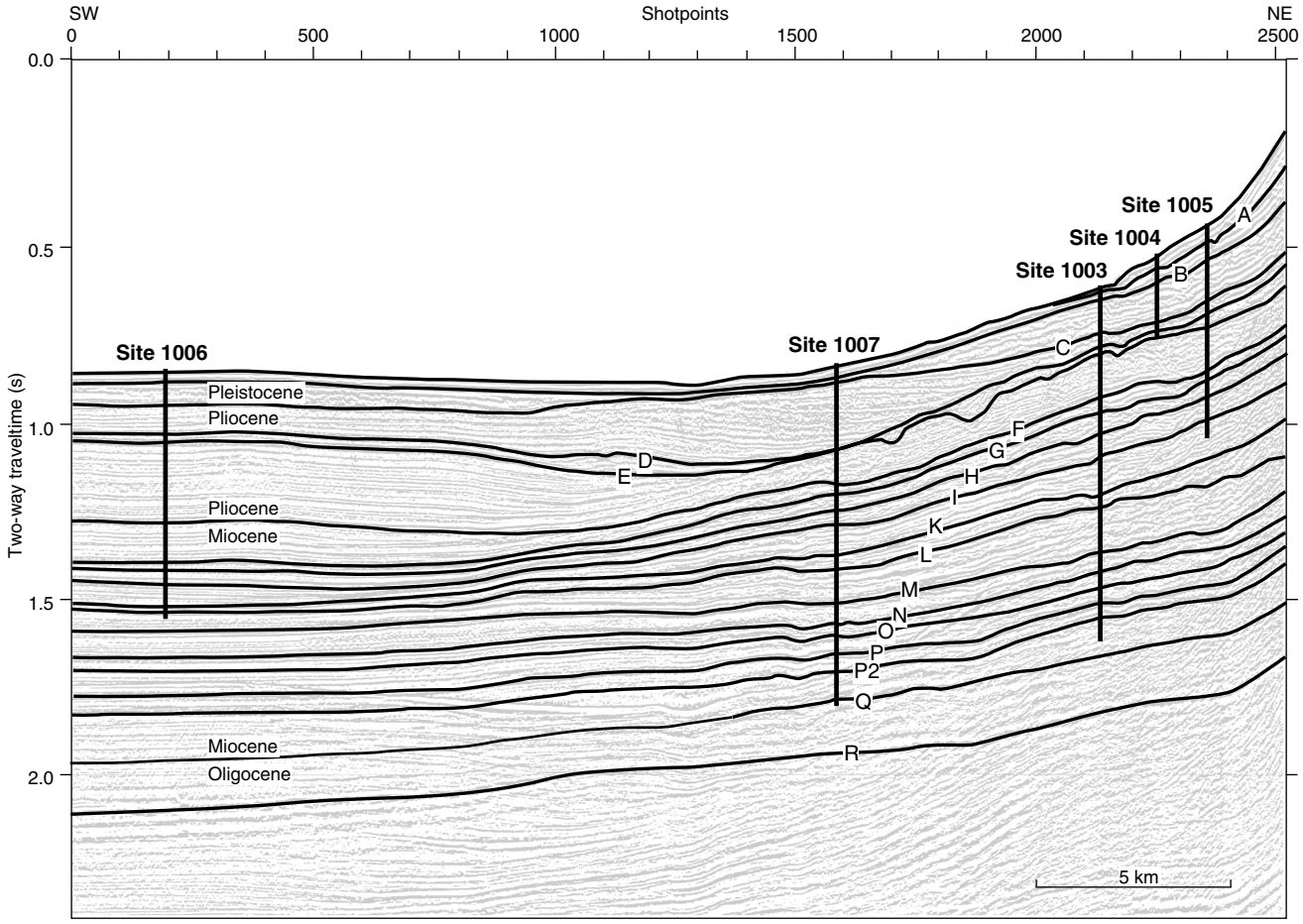

Figure 2. Portion of the high-resolution multichannel seismic Line 106 that retraced the cross-bank Western Geophysical seismic line with the positions of Sites 1003, 1004, 1005, and 1007. Site 1006 was positioned on a thick, continuous sequence of Neogene-aged drift deposits. These deposits onlap and interfinger with prograding bank deposits (from Shipboard Scientific Party, 1997a).

Data quality assurance (QA) was monitored by concurrent measurement of elemental concentrations in quality control (QC) U.S. Geological Survey (M-series and T-series) Standard Water Reference Samples (SWRS), certified reference materials from NRC Canada, and/or by analysis of IAPSO standard seawater. Agreement was always within the limits of the statistical range of the certified or recommended reference values and within the expected instrumental precision for the method utilized (3%–5% relative).

RESULTS

Minor and trace element concentrations (Ba, Fe, Li, Mn, Sr, and Rb) determined in our laboratory are presented in Table 1.

Dissolved Sr^{2+} concentrations determined on board the *JOIDES Resolution* by atomic absorption spectrometry (AAS) with a N_2O/C_2H_2 flame were compared with shore-based ICP/OES data for IW samples from Sites 1005 and 1006. Differences between the data sets are generally well below 10% relative, except for a few samples. Because of the remarkable agreement between the two methods, IW samples from Site 1007 were not analyzed for Sr^{2+}, and discussions are based on shipboard data. Discussions of other trace pore-water constituents are based on shore-based results.

Significant differences exist, however, between the shipboard and shore-based Li^+ data (Fig. 3), and their cause is explored in the discussion section.

Shore-based determinations of Fe^{2+} also show considerable deviation from the shipboard data (Fig. 4). Concentrations of Fe^{2+} determined aboard the *JOIDES Resolution* by flame atomic absorption spectrometry (FAAS) are higher than those determined in our laboratory by ICP/OES. The differences reach up to an order of magnitude for some of the lower concentration samples. The greatest deviations between shipboard and shore-based Fe^{2+} determinations were observed in IW from Site 1007. The most noticeable differences occur in the shallower sections of the hole, where the marked concentration increase with depth observed in the shipboard analyses is not evident in the shore-based data. Additionally, none of the large dissolved Fe^{2+} spikes observed in shipboard data exist in the shore-based data.

Results of shore-based spectrometric determinations of dissolved Mn^{2+}, Rb^+, and Ba^{2+} are also given in Table 1. Dissolved Mn^{2+} data in Table 1 are primarily results from FIA determinations on 0.2-µm-filtered trace metal splits, except below 400 mbsf at Site 1005 and below 340 mbsf at Site 1006. FIA results are presented wherever available. Although reasonable agreement was generally observed between Mn^{2+} data obtained by ICP/OES and FIA when concentrations exceeded 150 nM, FIA results are more reliable because of the greater sensitivity and accuracy of the latter technique, which includes a matrix elimination step. Because trace metal splits were not available below 400 mbsf at Site 1005, however, results of ICP/OES analyses of alkalinity splits are presented. All Mn^{2+} data at Site 1006 are from trace metal splits, however, samples below 340 mbsf were only analyzed by ICP/OES. Thus the data presented in Table 1 and shown in Figure 5 represent a combination of FIA and ICP/OES analyses. Dissolved Rb^+ was only determined in IW from Site 1106; the depth profile is presented in Figure 6. Dissolved Ba^{2+} profiles (Fig. 7) exhibit large fluctuations within each hole as well as between sites. The low-

Table 1. Minor and trace elements in interstitial water from Sites 1005–1007, as indicated by shore-based data.

Core, section, interval (cm)	Depth (mbsf)	Li (μM)	Rb (μM)	Sr (μM)	Ba (μM)	Fe (μM)	Mn* (nM)
166-1005A-							
1H-1, 145-150	1.4	25.9		98	0.1	0.55	66
2H-1, 145-150	4.0	27.2		102	0.1	1.79	62
2H-3, 140-150	6.9	27.7		107	0.1	1.17	67
2H-5, 140-150	9.9	30.1		103	0.0	0.84	72
3H-1, 140-150	13.4	31.4		103	0.0	0.71	>350
4H-5, 140-150	23.4	29.0		130	0.2	1.54	70
5H-5, 140-150	32.9	29.0		107	0.1	0.25	40
6H-5, 140-150	42.4	28.4		160	0.3	5.13	60
7H-4, 140-150	50.4	31.3		409	0.4	0.36	94
8H-4, 140-150	57.9	37.5		673	0.3	1.91	89
9H-5, 135-150	68.0	44.1		777	0.3		69
10X-1, 135-150	68.9	45.8		894	0.4	0.18	30
11X-1, 135-150	73.4	49.4		1006	0.5	0.05	26
12X-4, 135-102	87.4	51.6		1072	0.5	0.07	174
13X-2, 135-150	94.0	51.9		1267	0.5		53
16X-2, 135-150	122.2	43.5		1241	0.6	0.16	98
19X-2, 135-150	150.2	65.5		1024	1.1	0.89	134
20X-5, 135-150	164.0	71.2		988	1.0	1.09	
22X-2, 135-150	178.0	76.8		1109	0.8	0.63	131
30X-3, 135-150	253.6	85.1		2722	1.1	0.95	<10
34X-2, 135-150	283.2	79.7		3402	1.8	0.36	162
35X-2, 135-150	289.4	85.0		3641	2.1	1.29	151
36X-2, 135-150	299.0						838
38X-1, 135-150	316.0	78.1		4046	3.8	0.89	1793
166-1005C-							
1R-1, 140-150	388.0	51.3		1303	0.3	2.58	204
5R-2, 0-8	425.5	51.4		627	0.3	6.08	347
9R-1, 0-10	460.7	53.1		632	0.3		53
12R-2, 0-10	490.0	47.2		576	0.4	13.73	445
16R-2, 0-10	526.8	50.3		611	0.1	2.04	171
20R-2, 124-135	564.9	63.4		743	0.2	10.64	371
24R-2, 50-58	601.0	68.7		777	0.4	13.63	323
28R-1, 102-111	637.0	65.4		716	0.2	5.09	183
33R-2, 0-11	683.4	72.6		1178	0.5	6.55	588
166-1006-							
1H-2, 143-150	2.9	27.8	1.56	152	0.2		1790
1H-4, 128-135	5.8				0.2	4.60	1850
2H-2, 143-150	10.0	28.1	1.49	162	0.1	0.09	84
2H-5, 143-150	14.5	29.1	1.57	188	0.1	0.27	255
3H-2, 143-150	19.5	29.2	1.74	212	0.2		196
3H-5, 143-150	24.0	29.5	1.60	282	0.3		177
4H-2, 140-150	29.0	29.4	1.47	435	0.2	8.08	118
5H-2, 140-150	38.5	28.5	1.52	705	0.3	1.78	116
6H-2, 140-150	48.0	28.8	1.50	786	0.4	1.97	132
7H-2, 140-150	57.5	29.1	1.45	992	0.4	0.89	149
8H-2, 140-150	67.0	28.7	1.44	1251	1.8	9.73	333
9H-2, 140-150	76.5	29.1	1.50	1346	0.6	1.19	154
10H-2, 140-150	86.0	29.5	1.37	1521	0.6	1.01	145
11H-2, 140-150	95.5	28.4	1.44	1778	0.7	2.42	141
12H-2, 140-150	105.0	30.3	1.44	1642	0.6	2.62	178
13H-2, 140-150	114.5	31.3	1.40	1912	0.7	0.45	93
14H-2, 140-150	124.0	32.0	1.45	2148	0.7		86
15H-2, 140-150	133.5	31.0	1.36	2237	0.9	0.16	167
16H-2, 140-150	143.0	29.8	1.33	2526	1.1	0.19	92
17H-2, 140-150	152.5	31.5	1.32	2632	1.2	0.23	160
18H-2, 135-150	162.0	30.3	1.37	2879	1.4	0.83	131
19H-2, 135-150	171.5	32.8	1.42	3164	2.0	0.18	67
20H-2, 135-150	181.0	30.8	1.37	3287	2.6	0.81	116
21H-2, 135-150	190.5	36.2	1.42	3471	4.0	0.83	91
22H-2, 135-150	200.0	35.1	1.38	3799	10.1	0.47	108
24H-2, 135-150	219.0	34.6	1.39	4122	30.0	0.74	109
26H-2, 135-150	238.0	33.7	1.33	4329	35.1	6.10	182
28H-2, 135-150	257.0	38.5	1.40	4603	38.7	2.66	123
30X-2, 135-150	276.0	46.4	1.35	4864	43.4	6.86	183
32X-2, 135-150	287.6	52.0	1.37	4605	43.8	5.07	366
34X-2, 135-150	306.0	60.5	1.40	5248	56.2	2.84	257
35X-2, 135-150	315.3	56.9	1.36	5466	58.4		291
38X-2, 135-150	342.7	76.9	1.73	6014	71.7	2.22	260
41X-2, 135-150	370.2	68.4	1.54	5981	91.9	2.35	335
44X-2, 135-150	397.6	77.5	1.74	6228	117.2	2.30	277
47X-2, 135-150	425.7	88.2	1.98	6397	155.2	1.71	299
50X-2, 135-150	453.0	94.9	1.93	6577	205.9	1.42	142
53X-2, 135-150	481.0	103.4	1.90	6214	227.8	1.08	204
56X-5, 135-150	512.8	123.9	2.08	6783	185.6	1.41	284
59X-2, 135-150	537.2	129.2	2.04	6579	160.0	1.53	414
62X-2, 135-150	566.1	136.8	2.15	6306	58.8	1.27	914
65X-2, 135-150	595.0	152.3	2.26	6335	153.6	1.70	336
68X-4, 135-150	626.9	169.3	2.42	6409	213.6	1.51	278
72X-5, 135-150	666.9	158.6	2.48	5414	43.3	1.01	220
75X-2, 135-150	691.3	161.0	2.33	4403	8.9	1.51	318
77X-2, 135-150	710.6	171.6	2.28	5100	48.4	6.38	2309
166-1007B-							
1H-4, 140-150	5.9	30.0			2.9	0.29	149
1H-6, 145-150	9.0	29.4			1.4	0.27	111
2H-2, 140-150	12.4	36.4			1.1	0.18	49
2H-4, 140-150	15.4	34.0			1.5		78
3H-2, 140-150	21.9	28.8			0.4	0.41	112
4H-5, 140-150	35.9	31.8			1.2	0.73	115
5H-5, 140-150	47.4	39.0			1.1		139
6H-3, 140-150	53.9	42.6			1.2	0.33	57
7H-5, 140-150	64.9	46.0			0.7	0.31	39
8H-4, 135-150	72.8	46.7			1.2	0.33	<25
9H-4, 140-150	82.4	48.0			0.9		109
10H-2, 140-150	87.6	51.7			1.1		83
11X-3, 140-150	96.1	54.0			0.8	0.04	77
15X-5, 140-150	136.9	61.1			0.3	0.42	78
16X-3, 135-150	142.8	62.5			0.3	0.21	54
17X-4, 135-150	153.2	62.4			0.4	0.41	130
18X-2, 0-15	158.3						127
23X-4, 135-150	209.0	70.2			0.4	0.30	160
24X-5, 135-150	219.8						
25X-5, 135-150	228.8	68.7			0.4	0.35	111
26X-5, 135-150	238.0	69.3			0.3		110
27X-5, 135-150	247.2	69.0			0.3	0.30	143
28X-3, 135-150	253.4						67
29X-1, 135-150	259.8	67.4			0.1	0.04	62
30X-2, 135-150	270.6	69.0			0.5	11.28	>240
38X-1, 0-11	341.1	62.1			0.2	2.58	163
166-1007C-							
6R-2, 0-10	351.4	57.8			0.4	2.17	193
12R-2, 123-135	409.8	76.9			0.1	0.09	51
17R-6, 99-114	463.3	82.1			0.2	1.83	122
19R-3, 134-145	479.1	82.4			0.4	12.78	112
21R-2, 130-142	497.0	82.3			0.5	6.52	113
24R-5, 136-144	530.4	98.1			0.9	6.57	91
26R-6, 105-121	549.4	102.6			2.0	3.83	61
28R-3, 103-116	565.3	97.8			2.7	9.53	50
31R-6, 105-121	597.5	102.7			3.8	3.55	126
34R-1, 135-152	620.8	106.7			10.2	0.65	105
37R-1, 0-12	648.3	103.4			12.0	0.63	55
40R-4, 139-150	682.2	111.9			11.6	0.76	95
45R-2, 0-12	726.7	110.2			20.1	1.68	115
47R-2, 0-14	745.7	106.6			30.9	2.77	
49R-2, 112-124	766.3	120.7			37.6	4.82	112
52R-2, 31-44	794.4	100.3			15.5	1.76	
57R-2, 0-10	842.1	147.2			25.3	2.07	82
60R-1, 98-113	870.5	154.4			27.0	1.62	
62R-2, 0-13	890.1	174.0			10.5	2.86	
66R-2, 28-39	929.0	249.4			68.3	2.70	

Notes: * = Mn data from flow injection analysis except as noted below; see text for additional details. Site 1005 ICP/OES data from alkalinity splits beginning with R cores (388 mbsf and below), Site 1006 ICP/OES data from trace metal splits beginning at Core 24H (219 mbsf and below).

est Ba^{2+} concentrations occur at Site 1005, whereas the greatest Ba^{2+} enrichments are in IW from Site 1006.

DISCUSSION

Profiles of minor and trace dissolved constituents are shown in figures with the following order: Site 1005, Site 1007, and Site 1006. This presentation is designed to place the profiles in a geographical context from east to west along the western margin of the GBB (Fig. 1). Site 1005, the easternmost and most proximal Bahamas Transect site on the edge of the platform, penetrates downlapping prograding sediments, whereas Site 1006 is the westernmost site and penetrates a more pelagic sediment sequence (see Fig. 2) in the northern portion of the Santaren Channel (Fig. 1). Site 1007 is intermediate to the other two (Eberli, Swart, Malone, et al., 1997). Discussion of the results will follow this format.

Analytical Chemistry

Lithium

Absolute and relative differences between the concentrations of dissolved Li^+ determined aboard the *JOIDES Resolution* and in our laboratory are plotted as a function of depth downhole in Figure 8. From a purely analytical standpoint, and in the absence of gross calibration errors, discrepancies in the data sets can arise from either in-

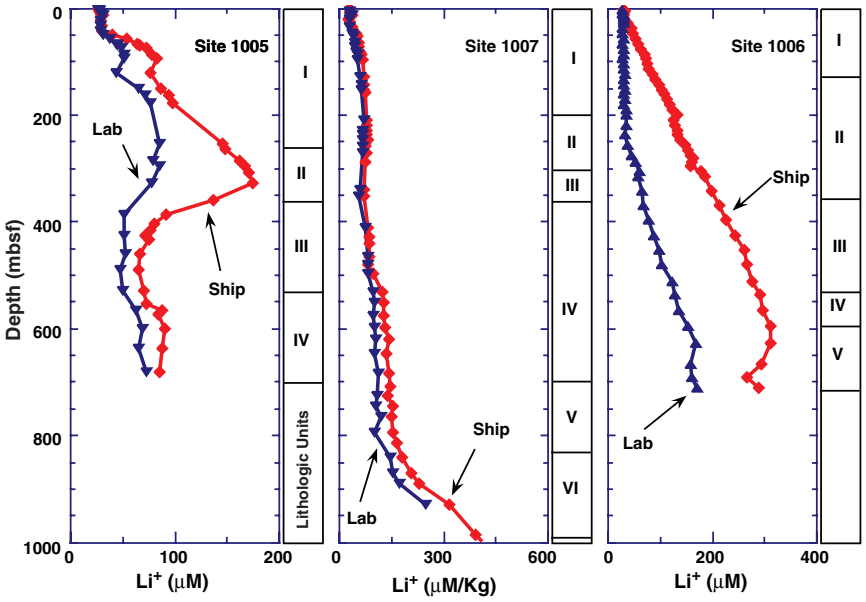

Figure 3. Comparison of shore-based and shipboard depth profiles of dissolved Li^+ at Bahamas Transect Sites 1005–1007.

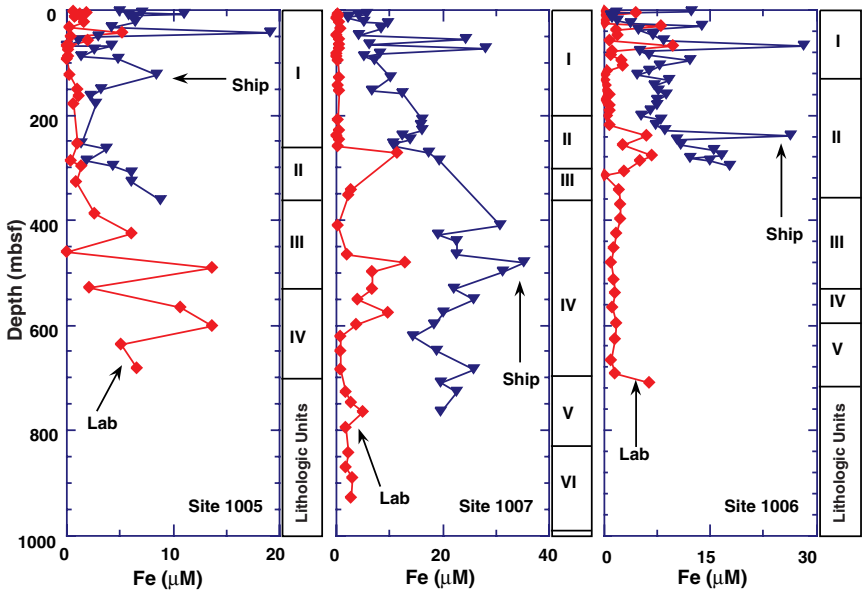

Figure 4. Comparison of shore-based and shipboard depth profiles of dissolved Fe at Bahamas Transect Sites 1005–1007.

adequate matrix matching of samples and calibration standards or insufficient background correction during the shipboard measurements. Shipboard standards for Li^+ determinations were prepared in seawater in an attempt to match the matrix of the IW samples. As described in the methods section, shore-based analyses were performed by AES with calibration by the method of standard addition and with offline emission measurements to correct for background. The latter allows us to correct effectively broad band emission from the matrix, as well as ionization interference effects that are often encountered with alkali metal analysis by flame atomic spectrometry.

We initially suspected that the shipboard analytical problems resulted from increased salinity of pore fluids downhole and the inability of the Varian AAS instrument to deal with the concomitant large increase in background signal. However, no simple relationship is apparent in Figure 8 between depth (i.e., salinity) and Δ-Li, suggesting that increased salinity is not solely the cause of the problem. Rather, other chemical species, likely nonconservative IW constituents, may be responsible for the observed discrepancy. The greatest relative and absolute differences between the two data sets occur in samples from Site 1006 (Fig. 8). At this site the greatest relative difference is observed in IW that displays total SO_4^{2-} depletion (~200 mbsf). The greatest absolute deviation, however, occurs in samples recovered near 450 mbsf. This depth corresponds to the NH_4^+ and (second) broad alkalinity maxima. In samples from Site 1005, differences are intermediate to those observed at Sites 1006 and 1007; however, the largest discrepancy also occurs in samples collected near the NH_4^+ and alkalinity maxima. At all three sites, the greatest absolute difference between the two data sets occurs in samples with the highest dissolved Sr^{2+} concentrations. This is consistent with the known problem of SrOH broad band emission causing an interference on the Li 670.8-nm line (Heinrichs and Herrmann, 1990). The general covariance between the shipboard dissolved Li^+ and Sr^{2+} profiles (Eberli, Swart, Malone, et al., 1997) also suggests strongly that the latter is responsible for the analytical interference, although a plot of shipboard determinations of Li^+ vs. Sr^{2+} (not shown), while generally linear, shows significant deviations that suggest that another source of interference also exists in the shipboard analyses. The occurrence of significant alkalinity and NH_4^+ maxima where large analytical discrepancies in Li^+ determinations were observed may simply be coincidental and reflect the fact that such conditions lead to enhanced

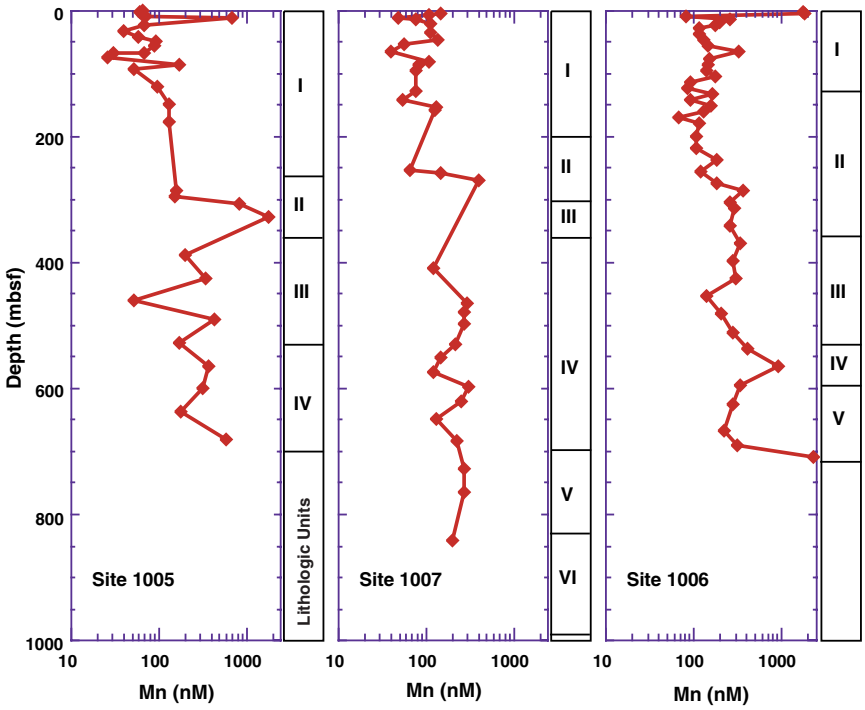

Figure 5. Depth profiles of dissolved Mn^{2+} at Bahamas Transect Sites 1005–1007.

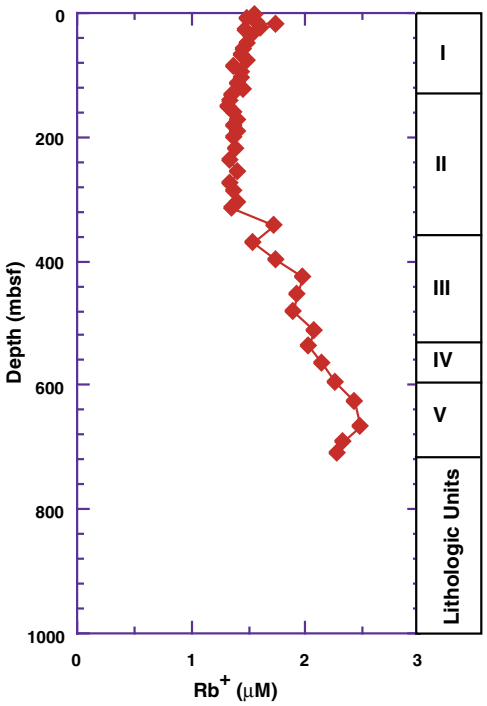

Figure 6. Depth profile of dissolved Rb^+ at Site 1006.

dissolution of aragonite, which is the primary Sr^{2+} carrier in sediments from the GBB. Nonetheless, molecular species (e.g., $NH4^+$) are well known to produce broad absorption and/or emission bands.

Although it appears that other species may contribute to the increased background signal, because IW recovered during Leg 166 exhibits the highest Sr^{2+} concentrations observed in ODP to date, Sr^{2+} likely contributed most to the observed analytical problems. Nonetheless, it is clear that care must be taken to account for large variations in any species likely to produce broad band absorption/emission when conducting Li^+ determinations aboard the *JOIDES Resolution*.

Iron and Manganese

Some important differences exist in the sample handling and analytical procedures used for determinations of dissolved Fe and Mn^{2+} in our laboratory and onboard the *JOIDES Resolution*. These differences likely contribute to a large extent to the differences observed between shipboard and shore-based data (Fig. 4). First, splits left over from shipboard alkalinity titrations were sealed in plastic tubes with pliers and subsequently cut open for FAAS analysis using scissors or a carpet knife. Whenever available, samples analyzed in our laboratory by ICP/OES and FIA were taken from Nalgene HDPE bottles that had been filled with sample under the laminar hood aboard ship and preserved with ultra-high purity HNO_3. Second, splits analyzed onboard the *JOIDES Resolution* were filtered through 0.45-µm acrodiscs, whereas those collected for shore-based studies were filtered through 0.2-µm acrodiscs.

Some of the difference between the two data sets is attributable to contamination of the shipboard samples with Fe during handling (alkalinity titration and subsequent storage and reopening of tubes). Because Fe is also notorious for existing as colloidal particles in natural waters, filtration through 0.2-µm acrodiscs likely removed a substantial portion of the larger colloidal particles. Thus, data from shore-based determinations of Fe in trace element splits are more representative of the dissolved fraction, and some of the difference between shipboard and shore-based results can be attributed to filtration effects. In spite of these important differences, the general trends defined by the shipboard data sets still correlate somewhat with those defined by shore-based determinations, albeit only crudely so.

Insufficient IW was recovered from whole-round core samples collected below 400 mbsf at Site 1005 to acquire trace metal splits; thus, the stored alkalinity splits that were not analyzed aboard the *JOIDES Resolution* were analyzed on shore for their dissolved Fe^{2+} and Mn^{2+} content. The transition trace metal data from these samples are, therefore, subject to a high bias because of potential contamination (i.e., Fe and to a lesser extent Mn), as described above, and filtration effects. However, shore-based determinations of dissolved Fe yielded significantly lower concentrations than those measured aboard the *JOIDES Resolution*. It is likely that the shore-based analyses were not as adversely affected by matrix effects. Also, because ICP/OES is more sensitive than AAS for many elements, dilutions of

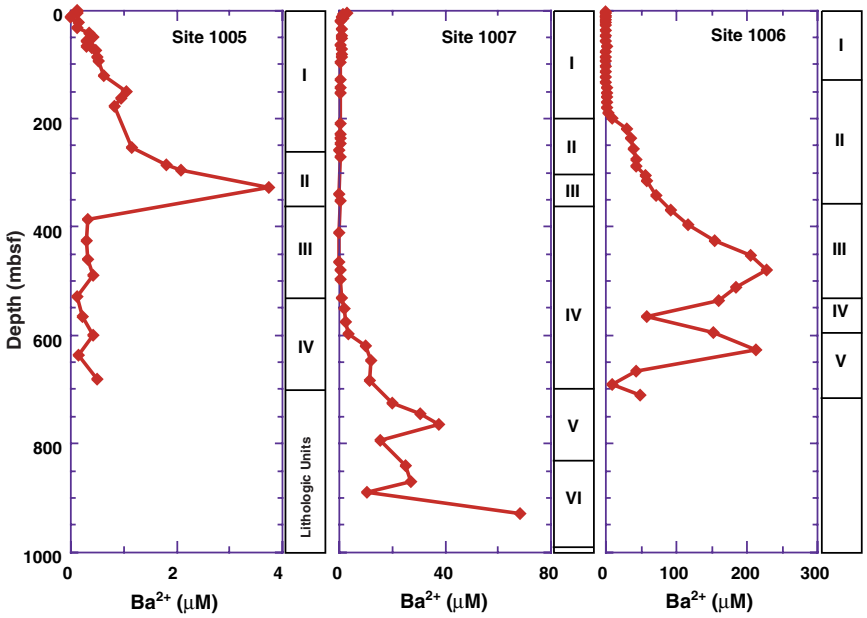

Figure 7. Depth profile of dissolved Ba^{2+} at Bahamas Transect Sites 1005–1007.

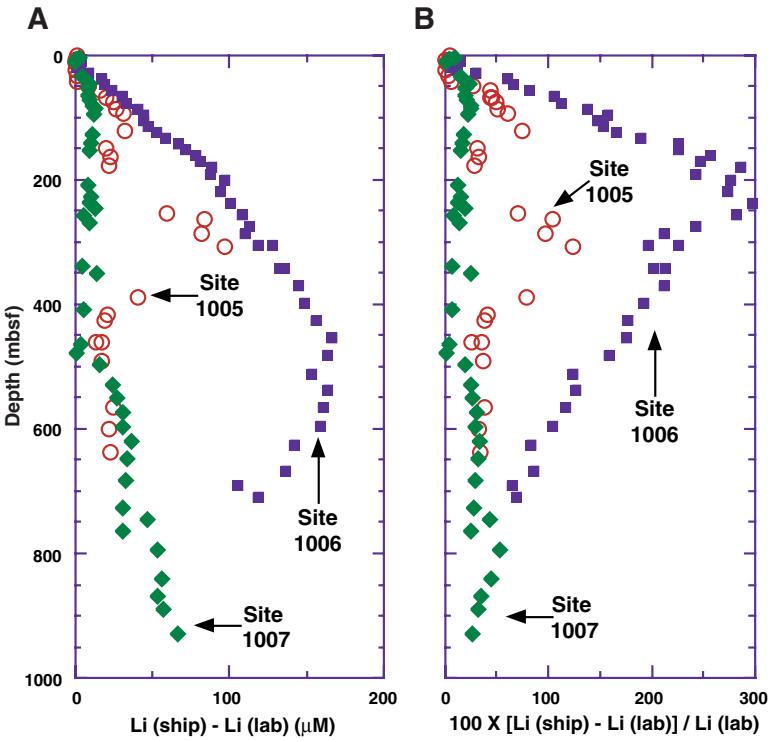

Figure 8. Differences in dissolved Li^+ concentrations as a function of depth for Bahamas Transect Sites 1005, 1006, and 1007. **A.** Absolute (µM) deviations. **B.** Relative (%) difference.

the samples analyzed by ICP/OES were possible, which substantially reduced matrix effects. Furthermore, offline background correction is used in ICP/OES, thereby minimizing matrix interferences and further increasing the reliability of the analyses. Thus, the shore-based analyses of the alkalinity split residues are deemed more reliable than their shipboard counterparts.

Geochemical Controls on the Composition of Pore Water

Lithium

The profiles shown in Figure 3 reflect a mediation of dissolved Li^+ concentrations by early diagenesis and by local lithological control at the various Bahamas transect sites. At Site 1005, a series of zones, which correspond well to lithologic units and to the chemical reaction zones identified during Leg 166 (Eberli, Swart, Malone, et al., 1997), display either invariant concentrations or positive or negative Li^+ gradients. The dissolved Li^+ profile covaries with several nonconservative dissolved constituents (e.g., alkalinity, NH_4^+, Sr^{2+}) in selected parts of the sediment column and mirrors remarkably the dissolved SO_4^{2+} profile (Fig. 9). Where the Li^+ profile does not appear to covary with those of other dissolved constituents, breaks in concentration gradients occur at the same depth and reflect stratigraphic horizons (i.e., physical barriers) that affect lateral fluid flow and inhibit the establishment of smooth vertical diffusive profiles. For example, the upper 40 mbsf displays relatively invariant profiles of many IW constituents. This section was interpreted to represent a flushed zone throughout which seawater flows freely and maintains near-seawater concentrations of conservative and most nonconservative IW constit-

uents (Eberli, Swart, Malone, et al., 1997). Dissolved Li^+ concentrations display, nonetheless, small but significant changes in this interval. Between ~50 and 100 mbsf in lithologic Subunit IA of Site 1005, dissolved Li^+ and several other constituents increase in concentration as SO_4^{2+} (Fig. 9) becomes strongly depleted during the bacterially mediated oxidation of organic matter (Claypool and Kaplan, 1974).

Conditions of high alkalinity and lowered pH favor the recrystallization of metastable aragonite and high magnesian calcite. These phases typically release trace elements upon dissolution (e.g., Baker, 1986; Baker et al., 1982). Thus, it is tempting to invoke biogenic carbonate as the primary source of Li^+ to pore fluids. The general shape of the Sr^{2+} and Li^+ profiles appears similar throughout large portions of the sediment column (Eberli, Swart, Malone, et al., 1997) and supports this inference, although greater deviations exist between the profiles of these constituents at Site 1007.

At Site 1005, dissolved Li^+ concentrations increase sharply within partially lithified and dolomitized sediments of Subunits IB and lithified sediments of Subunit IC, consistent with expulsion of Li^+ from solid phases during carbonate recrystallization reactions that formed the lithified intervals. Also, the lower dissolved Li^+ concentrations below 260 mbsf in the less lithified sediments of Units II and III may reflect a much-decreased rate of diagenesis of biogenic carbonate and concomitant release therefrom. Reduced microbial activity in this interval is evidenced by a return of elevated SO_4^{2-} concentrations, which approach seawater values below 500 mbsf. Deeper downhole, the dissolved Li^+ profile largely parallels that of Sr^{2+}, and a final change in the Li^+ gradient below ~525 mbsf also coincides with depletion of SO_4^{2-}.

Despite the qualitative correlation between dissolved Li^+ and Sr^{2+} profiles described above, the proposed exclusion of Li^+ during recrystallization of metastable carbonate minerals in the sediments cannot account for all of the observed increases in concentration downhole. For example, if we were to assume a conservative behavior for Li^+, just the increase in salinity downhole at Site 1005 could account for approximately half the observed increase in dissolved Li^+ above the normal seawater concentration. Furthermore, dissolved Li^+ and Sr^{2+} do not covary that strongly. This is especially true in the uppermost portion of the sediment column. Quite sharp variations in the dissolved Li/Sr value occur as a function of depth in the upper 20 m of sediments at Sites 1005 and 1007 (Fig. 10). Clearly different processes must govern their behavior here. The dissolution of biogenic silica may release Li^+, at least in the shallowest sediments (e.g., Gieskes, 1983; De Carlo, 1992, and references therein). Indeed, in the range of 15–20 mbsf at Sites 1005 and 1007 and between 122 and 164 mbsf at Site 1005, concentrations of Li^+ and SiO_2 in pore water increase, whereas that of Sr^{2+} does not.

Reactions involving biogenic silica, however, are unlikely to explain the Li^+ distribution in deeper sediments. The same can likely be said for diagenetic reactions of aragonite. Rather, a possible mechanism for the release of Li^+ to solution is by ion exchange with NH_4^+. At all GBB sites, there is a notable coincidence of high dissolved Li^+ concentration with the zones displaying high NH_4^+ concentrations. This is particularly true deeper downhole, where acid insoluble residues, interpreted here to represent largely detrital matter, tend to be more abundant than in the shallower portions of the holes. Examination of Figure 10 reveals features that are consistent with these inferences. For example, the Li/Sr value decreases substantially at Site 1007 below 450 mbsf, probably because of an increase in the abundance of aragonite in the sediments that are a source of Sr^{2+}. The interval between ~200 and 500 mbsf, where the Li/Sr value is highest (except for that in the uppermost 50 mbsf), contains abundant detrital minerals (e.g., clays) (Eberli, Swart, Malone, et al., 1997) that represent a potentially more important source of Li^+ in this hole. The substantial drop in the Li/Sr value below 475 mbsf, although coinciding with a zone still containing significant quantities of detrital minerals, occurs where aragonite is sufficiently abundant that its recrystallization could also supply the pore water with dissolved Sr^{2+}. Further support for a terrigenous/detrital source material for Li^+ is found near the bottom of the hole where the abundance of terrigenous/detrital minerals, as determined on the basis of weak acid-insoluble residues, increases sharply and an increase in the Li/Sr value is observed.

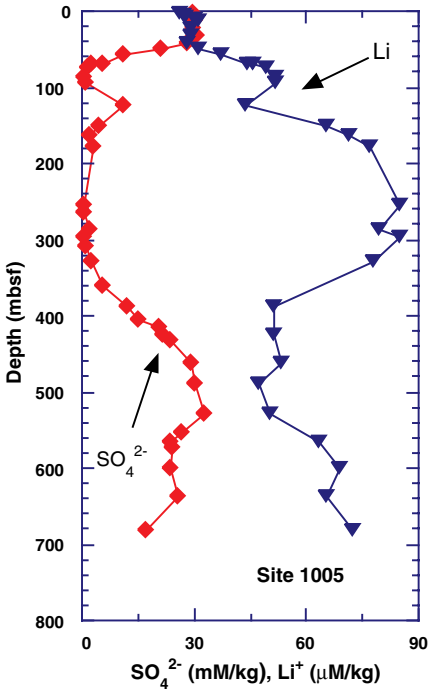

Figure 9. Depth profile illustrating antithetical correlation between dissolved Li^+ (solid diamonds) and SO_4^{2-} (solid triangles) at Site 1105.

It should also be borne in mind that the low solubility of $SrSO_4$ exerts a strong control on the abundance of dissolved Sr^{2+} (e.g., Baker and Bloomer, 1988) and complicates the interpretation of the dissolved Li/Sr profiles shown in Figure 10. Solubility control by celestite should have the greatest influence at Site 1005, where pore fluids between 450 and 600 mbsf are near saturation with respect to this mineral (see fig. 24 in Shipboard Scientific Party, 1997b). Thus, the increase in the Li/Sr value below 400 mbsf is not entirely attributable to increases in dissolved Li^+ derived from terrigenous/detrital minerals. More abundant dissolved SO_4^{2-} in this interval (Fig. 9), especially near 500 mbsf, likely limits the concentration of dissolved Sr^{2+}. At Site 1007, dissolved SO_4^{2-} is also present near 475 mbsf, but at substantially lower concentrations than at the same depth in Site 1005. Thus, celestite solubility should not control dissolved Sr^{2+} in this depth interval nor should it influence the Li/Sr value.

The mediation of dissolved Sr^{2+} by celestite solubility becomes unimportant below 200 mbsf at Site 1006 because SO_4^{2-} is fully depleted. Thus, any changes in the Li/Sr value must result from differences in the sources of these two elements. Site 1006 is positioned on a continuous thick section of Neogene-aged drift deposits that interfingered with prograding sediments from the GBB (Eberli, Swart, Malone, et al., 1997). It is also characterized by a greater abundance of insoluble/detrital minerals throughout most of the sedimentary column than either Site 1005 or 1007. Sediments at Site 1007, however, contain a greater abundance of detrital minerals than those at Site 1005, even reaching greater concentrations in some sections than observed at Site 1006. Nonetheless, detrital minerals are most uniformly distributed throughout the sediments of Site 1006. Thus, this material can be invoked as a source of Li to the pore water. The Li/Sr value, however, always remains lower at Site 1006 than at Site 1005 and is lower than above 600 mbsf at Site 1007.

Variations in Li/Sr should be viewed with some caution when used as a tool to evaluate sources of these two elements. Exceptions

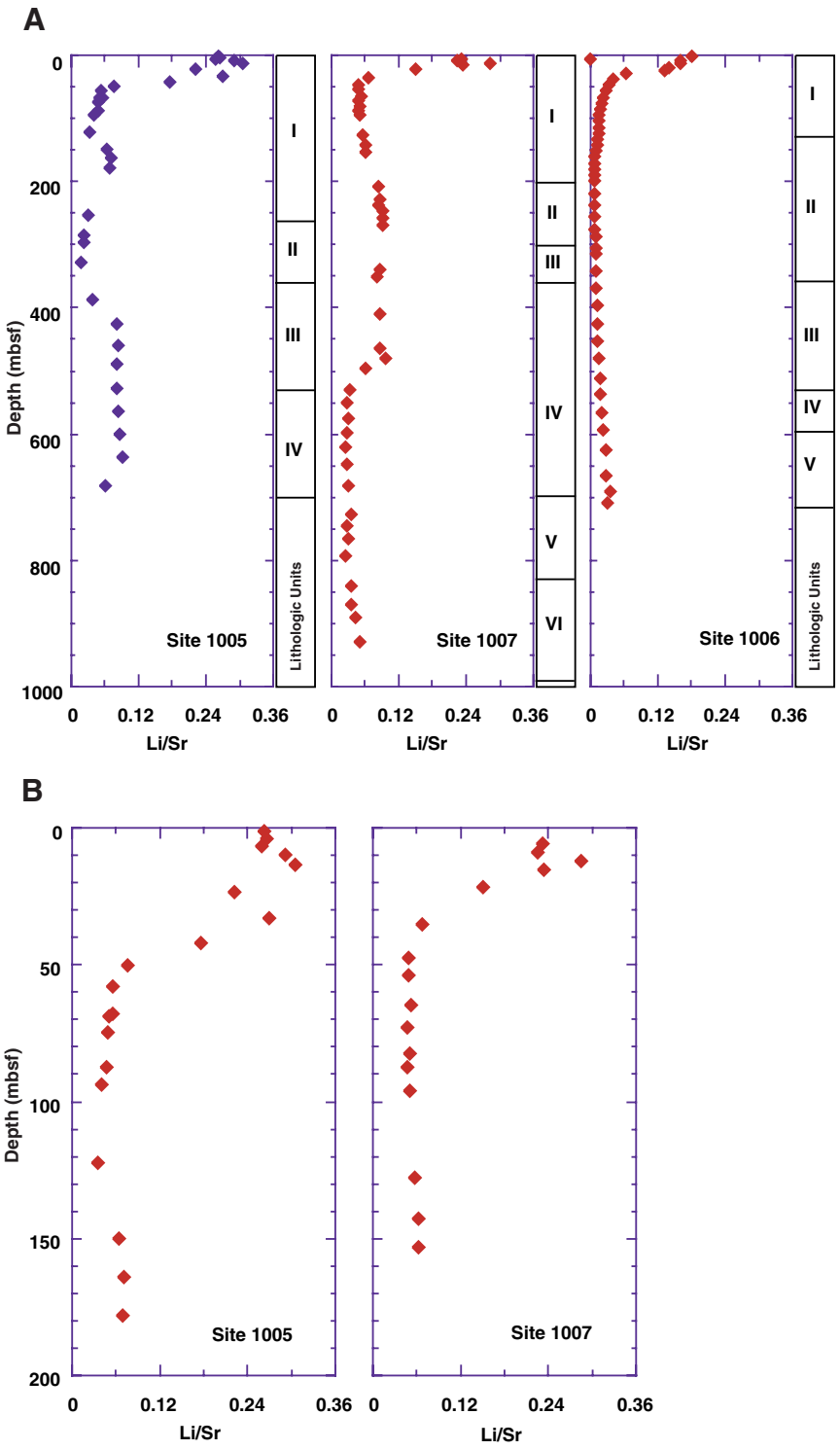

Figure 10. Dissolved Li/Sr ratio as a function of depth at Bahamas Transect Sites. **A.** Full stratigraphic column for Sites 1005–1007. **B.** Upper 200 mbsf of Sites 1005 and 1007.

include relatively anoxic sediments in the uppermost portions of the sediment column, where extreme changes in the Li/Sr value occur over relatively shallow depth intervals. Nonetheless, dissolved Li^+ can derive primarily from three sources: (1) early diagenesis of biogenic silica, (2) terrigenous material (especially clay minerals), and (3) exclusion during the recrystallization of carbonates. This is consistent with earlier suggestions by Froelich et al. (1991). A possible fourth source, which decreases in importance from Site 1005 to Sites 1007 and 1006, is simply the increased salinity of pore fluids that might contain correspondingly greater dissolved Li^+ with increasing depth downhole.

Hoefs and Sywall (1997) report that marine carbonates average 2 µg/g Li. De Carlo (1992) showed that sediments from the Exmouth Plateau that are rich in terrigenous matter contain 50–130 µg/g Li, whereas predominantly carbonate-rich sediments from this area often displayed <10 µg/g Li. Kabata-Pendias and Pendias (1992) compiled the Li content of various type soils and reported concentrations ranging from <1 µg/g to 130 µg/g for clay-rich soils from New Zealand.

The weak-acid soluble fraction of sediments from Site 1007 contains between 8 and 38 µg/g, with most samples exhibiting concentrations of <20 µg/g (P. Kramer, unpubl. data). The lower values are representative of predominantly biogenic carbonates of the GBB, whereas values greater than 15 µg/g Li usually occur in sediments from deeper than 600 mbsf. The latter must contain an important Li contribution from detrital minerals. This inference is supported by an increase in the amount of insoluble residues (terrigenous/detrital minerals) downhole, reaching 30–35 wt% in certain samples from below 1000 mbsf. These sediments likely contain interlayer Li bound in clay minerals, which can be released to solution by ion exchange with NH_4^+. Thus, even in sediments with substantially more biogenic silica and carbonate than terrigenous material, the Li contribution from terrigenous material could be proportionally greater than that from the biogenic components.

We calculate below the potential of the solid phase to contribute Li to the pore water of sediments from the GBB. Several assumptions are made to simplify this calculation. First, we assume that sediments recovered during Leg 166 contain ~25% terrigenous/detrital material by mass throughout all of Site 1006 and below 600 mbsf at Site 1007. Abundances are considerably lower at Site 1005 where we assume a <5%–10% contribution of terrigenous/detrital matter to the sediment. Second, we assume conservatively that terrigenous/detrital material contains 50 µg/g of potentially available Li and use a biogenic carbonate value of 2 µg/g Li. We further assume no significant contribution to dissolved Li^+ from biogenic silica, and an equal propensity of each of the two other phases for providing Li^+ to the pore fluids. Based on these assumptions, we calculate that the terrigenous fraction could contribute nearly 90% of the Li^+ throughout all of Site 1006 and below 600 mbsf at Site 1007. At Site 1005, the dissolved Li^+ contribution derived from detrital material could still reach 58%–74% of the total, depending on whether a 5% or 10% terrigenous contribution were considered.

A caveat to the above calculations regards whether terrigenous material has an equal propensity to release its Li to solution as does biogenic carbonate. Although terrigenous material is typically more resistant to solution than biogenic carbonates, because clay minerals are an important carrier of Li, have high surface areas, and readily exchange univalent cations, it is likely that Li bound in clays is readily accessible and, therefore, available for release to solution. This is particularly true where interstitial fluid concentrations of NH_4^+ are in the millimolar range. Additionally, a significant portion of the Li might have been originally associated with Fe- and Mn-rich phases which are readily solubilized, especially under the sub-oxic and anoxic conditions encountered at these GBB sites. Support for this inference comes from the observation that the Li content of the easily solubilized phases in sediments recovered deep within Site 1007 can reach more than 20 µg/g by 600 mbsf. Thus, we estimate that nonbiogenic phases at or below this depth can easily provide at least 50%, if not more, of the dissolved Li^+ to pore fluids.

Rubidium

Dissolved Rb^+ is a minor constituent (1.4 µM) of seawater and displays a conservative behavior in the oceans (Bruland, 1983). High-temperature seawater-rock interactions, however, are known to enrich Rb^+ in fluids up to several orders of magnitude above seawater concentrations (e.g., Mottl and Holland, 1978). Enrichment of this element in pore fluids of deep-sea sediments has usually been attributed to alteration of volcanic matter (e.g., Gieskes, 1983). For example, Mottl (1992) observed more than five-fold enrichment of Rb on conical seamount (Site 780), a serpentinite in the Mariana forearc. More recently, two- to nearly three-fold enrichments of dissolved Rb^+ over seawater were observed in pore water from Sites 998 and 999 (Sigurdson, Leckie, Acton, et al., 1997). These were correlated with the occurrence of volcanic ash layers and dispersed volcanic minerals within the sediments, indicating that low temperature alteration of such minerals in sediments also leads to enrichment of Rb^+ in pore fluids.

The dissolved Rb^+ concentration at Site 1006 (Fig. 7) reaches nearly twice the seawater value by 700 mbsf, yet pore fluids at all depths, except immediately below the mudline, are depleted on a chloride-normalized basis relative to a fluid with seawater proportions. Dissolved Rb^+ becomes increasingly more depleted relative to seawater as a function of depth in the upper 250 mbsf of the profile. The cause of this depletion remains elusive. Increases in dissolved Rb^+ and the Rb/Cl ratio occur only below ~320 mbsf. The very slight enrichment of Rb^+ immediately below the mudline may be an artifact derived from a temperature of squeezing effect as noted for K^+ in interstitial waters from the first 50 m of deep-sea sediments (Bischoff et al., 1970). Because volcanic matter is absent from sediments of the GBB, its alteration cannot be invoked to account for the increase in the concentration of Rb^+ downhole. A potential source of Rb^+ that might lead to enrichment in interstitial fluids is detrital matter (K. Lackschewitz, pers. comm.). Mineralogical analyses conducted during Leg 166 indicate a substantial increase in detrital matter below 300 mbsf at Site 1006. It is also interesting to note that the onset of dissolved Rb^+ enrichment coincides with the zone (300–420 mbsf) where dolomite was most abundant (Eberli, Swart, Malone et al., 1997). A submaximum in the dissolved Rb^+ profile exists at 420 mbsf. Thus, it is tempting to contemplate exclusion of Rb^+ from dolomite during carbonate recrystallization reactions to account for its enrichment. Such an input of Rb^+ to pore fluids further downhole, however, is unlikely as the abundance of dolomite decreases substantially below 420 mbsf, whereas the concentration of dissolved Rb^+ continues to increase. Because the abundance of detrital and clay minerals continues to increase and peaks just below 600 mbsf, it is more likely that this material is the source of the Rb^+ enrichment observed here. The slightly lower dissolved Rb^+ concentration observed in the two deepest samples supports this inference, because these samples also coincide with a lower abundance of detrital matter (Eberli, Swart, Malone, et al., 1997). Ostensibly Rb^+ may be introduced to pore water by a mechanism similar to that invoked for Li^+, i.e. ion exchange with NH_4^+ in clay minerals.

Barium

Throughout the sediments of the GBB, dissolved Ba^{2+} concentration increases wherever SO_4^{2-} becomes depleted (e.g., von Breymann, et al., 1992). This antithetical relationship is expected because the concentration of dissolved Ba^{2+}, much like that of Sr^{2+}, is mediated largely by the solubility of its sulfate salt. The source of Ba^{2+} to the pore water, however, is likely different than that of Sr^{2+}. The enrichment of dissolved Sr^{2+} in pore water from the GBB is caused primarily by its release from aragonite during early diagenesis and exclusion from the lattice during recrystallization of low magnesian calcite (e.g., Baker et al., 1982; Baker, 1986). The source of Ba^{2+} in sediments of the GBB, on the other hand, is more likely to be barite as well as detrital matter for the reasons explained below.

Barium concentrations can reach several thousand µg/g in carbonate-rich sediments (e.g., Boström and Backman, 1990; Schroeder et al., 1997) and sedimentary Ba has been used as a proxy for barite whose formation has been shown to be associated with biological productivity (Dehairs et al., 1980, 1987; Bishop, 1988; Francois et al., 1995; Paytan, 1995; Schroeder et al., 1997). However, Ba is abundant in many phases. Known associations exist between elevated Ba concentrations and hydrothermal mineralization (Bonatti et al., 1972), biogenic sediments/silica (Schmitz, 1987; Bishop, 1988), biogenic barite (Dehairs et al., 1987), and also terrigenous matter (De Carlo, 1992). Mixed sediments, however, can display highly variable concentrations of Ba. For example, De Carlo (1992) reported Ba contents of several hundred to a maximum of 9000 µg/g in hemipelagic

sediments of the Exmouth Plateau containing variable amounts of siliciclastic matter. Greater Ba concentrations generally correlated with greater siliciclastic contents, although certain carbonate- and silica-rich intervals also displayed high concentrations of Ba. In sediments from the Japan Sea, von Breymann et al. reported solid-phase Ba concentrations ranging from <300 µg/g to as high as 12.8 mg/g. The latter, along with the 13.2 mg/g reported by Schroeder et al. (1997) in equatorial sediments from Site 850 probably represent the highest observed Ba concentrations in sediments recovered during the Ocean Drilling Program. These studies demonstrate the variable nature of the Ba content of marine sediments; thus, depending on the depositional environment, several sources can be invoked to account for the release of Ba to pore fluids under anoxic conditions.

Three sources of Ba appear likely in sediments from the GBB: (1) the crystal lattice of biogenic carbonates, (2) barite derived from remineralization of biogenic/organic matter, and (3) Ba in detrital/terrigenous matter that generally comprises no more than ~25% of the sediment. A measure of the lattice-bound Ba content of biogenic carbonates can be evaluated from the fraction of the sediments from Site 1007 that is soluble in dilute acetic acid (P. Kramer, unpubl. data). In the upper 400 mbsf of the sediments, this fraction generally contains <20 µg/g Ba. Below this depth, however, readily solubilized Ba concentrations increase substantially to 50 µg/g by 800 mbsf, where detrital minerals represent <10% of the sediment, peak around 140 µg/g near 900 mbsf, where detrital minerals constitute ~10%–15% of the sediment, and then return to <50 µg/g in the interval from 1000 to 1100 mbsf (P. Kramer, unpubl. data). A sharp increase to over 150 µg/g Ba is observed near the bottom of the hole where the abundance of detrital minerals is ~20%–25% of the total. Based on these data, relatively pure biogenic carbonates contain no more than 20 µg/g Ba. Dissolution and recrystallization of this material under anoxic conditions could provide Ba^{2+} to pore fluids, if an exclusion mechanism such as that described for the release of Sr^{2+} from biogenic carbonates, is invoked. However, other sources must be more important.

Because complete dissolutions of sediments from GBB sites were not performed, the total Ba content of the sediments is not known and it is not possible to estimate how much Ba is present in the form of barite derived from remineralization of marine organic matter or organic matter associated with the terrigenous matter hypothesized to originate from Hispaniola and Cuba. Thus, it is not useful to attempt a calculation analogous to that described above for Li^+. There clearly is a greater propensity of detrital minerals than the lattice of carbonate minerals for providing the dissolved Ba^{2+} observed in pore water from the GBB sites. The observed 150 µg/g of releasable Ba from sediments deep in Site 1007 indicates that the easily solubilized component of these sediments can provide approximately seven times more Ba^{2+} to solution than can be derived from the lattice of carbonates. The covariance between weak-acid soluble Ba and Fe, and Mn to a lesser extent, in sediments from Site 1007 (P. Kramer, unpubl. data) implies that easily solubilized Fe and Mn containing minerals possibly associated with but much more reactive than other detrital minerals do comprise a significant source of Ba. Our observations are consistent with Schroeder et al. (1997), who found a strong correlation between Ba and both Fe and terrigenous accumulation in carbonate sediments of the deep equatorial Pacific Ocean, although the vast majority of Ba was associated with biological productivity. The covariance between dissolved concentrations of Ba and Fe and detrital mineral content observed here is much stronger than that for Li. At Site 1006, where sediments typically contain more detrital matter than at Sites 1005 and 1007, the absence of a correlation between dissolved Ba^{2+} and Fe is explained by the removal of the latter from solution and its sequestration in the sediments as pyrite, other metastable Fe-sulfides, or carbonate phases (Eberli, Swart, Malone, et al., 1997). Nonetheless, barite formed during remineralization of biogenic/organic matter, either in the water column or upon shallow burial diagenesis, likely remains the most important source of Ba to pore fluids of the GBB sites.

Manganese and Iron

Concentrations of dissolved Fe and Mn^{2+} (Table 1; Figs. 4, 5) are considerably lower than observed in many previously sampled deep-sea sediments (Gieskes, 1981; De Carlo, 1992; Mottl, 1992; Sigurdson, Leckie, Acton, et al., 1997, and references therein). The profiles from the GBB sites do not appear to closely follow the conventional redox sequence observed in shallow sediments associated with the degradation of organic matter. The subsurface enrichments of dissolved Fe and Mn^{2+} that are normally observed in pore fluids as more favorable terminal electron acceptors become depleted do not seem to be manifested strongly here. Only at Site 1006 is the subsurface maximum of Mn significant, yet it only reaches <2 µM. This is considerably lower than observed at many other DSDP and ODP sites, where dissolved Mn^{2+} concentrations of 20–80 µM are not uncommon.

The low concentrations of dissolved Mn^{2+} observed here compared to many other deep-sea sediments likely reflect a combination of the predominance of biogenic carbonate in the sediments of the GBB transect sites and rapid rates of microbial degradation of organic matter. The concentration of Mn^{2+} increases at each site, primarily deeper downhole, where noncarbonate minerals become more abundant. As expected from its redox chemistry, the intervals displaying higher concentrations of Mn^{2+} in these highly variable profiles occur principally where SO_4^{2-} becomes substantially depleted or in the anoxic portions of the holes (e.g., near 300 mbsf at Site 1105, below 200 mbsf at Site 1006, and below 450 mbsf at Site 1007). Even then, dissolved Mn^{2+} does not exceed 2 µM, except in the deepest sample analyzed from Site 1006.

Concentrations of dissolved Fe are also quite variable; they do not display clear subsurface maxima expected from a classical redox/electron acceptor sequence, yet show a general increase downhole. Throughout most of the sedimentary column, however, concentrations of Fe in the pore fluids remain approximately one order of magnitude lower than observed in many other deep-sea sediments (e.g., Gieskes, 1981; De Carlo, 1992; Sigurdson, Leckie, Acton, et al., 1997, and references therein). Dissolved Fe also increases substantially, as expected and in a manner similar to the behavior displayed by Mn^{2+}, wherever SO_4^{2-} becomes strongly depleted. Notable exceptions include the first SO_4^{2-} minimum at Site 1005 (near 316 mbsf) and below 250 mbsf throughout most of Site 1006. In these intervals, Fe has been mostly sequestered into the sediments by precipitation as pyrite, other metastable sulfides, or incorporation into carbonate minerals (Eberli, Swart, Malone, et al., 1997).

Clearly, the low concentrations of Mn^{2+} and Fe in interstitial water from GBB transect sites reflect high rates of microbial oxidation of organic matter in a system characterized by a low abundance of easily reduced Fe- and Mn-rich phases that can act as a source of these elements to the pore water. Peaks in the weak–acid extractable Fe and Mn in sediments of Site 1007 (P. Kramer, unpubl. data) coincide reasonably with the intervals showing more elevated concentrations of dissolved Fe and Mn^{2+}. The general correlation between the dissolved concentrations of these elements as a function of depth with the abundance of detrital minerals substantiates this inference.

Likely Fe-rich lateritic soils derived from the weathering of volcanics on Cuba and Hispaniola and carried by the northward currents are an important source of Fe and Mn. Their occurrence in alternating layers throughout the sediments of the GBB is consistent with changing sea level, possibly in a periodicity of low-amplitude Milankovitch cycles. Another potential source of detrital minerals, although of a more constant nature, is an aeolian input of African dust carried across the Atlantic (e.g., Duce et al., 1991; Prospero, 1996).

Fluctuations in sea level influence the delivery of biogenic carbonates to the GBB transect sites. Higher productivity on the Bahamas platform during sea-level highstands leads to a dilution of aeolian inputs by abundant biogenic carbonate. Conversely, the aeolian contribution becomes proportionally more important during sea-level

lowstands, and the detrital fraction of the sediment from such intervals can provide a source of Fe and Mn to pore fluids during diagenesis. Aeolian dust has been reported to be more soluble than typical detrital matter and may release up to 10% of its Fe content because of an enhanced solubility imparted by chemical alteration during its atmospheric transport (Duce et al., 1991). This solubilization, however, is kinetically rapid and, whatever its extent, it is unlikely to be of great importance in pore waters whose composition has evolved over tens of thousands to millions of years.

In comparison with dissolved Ba^{2+}, however, concentrations of Mn^{2+} and Fe in interstitial water remain much lower than might be predicted on the basis of their abundance in the readily solubilized minerals (and likely more so in the more refractory minerals) present in the sedimentary column. For example, readily solubilized Ba and Mn in sediments of Site 1007 vary within a similar range of a few to ~200 µg/g, whereas the Fe range is approximately one order of magnitude greater. The concentrations of dissolved Ba^{2+} fluctuate from 10 µM to nearly 80 µM in the anoxic sediments of Site 1007 (they are substantially higher, 10–228 µM, in anoxic sediments of Site 1006). Concentrations of dissolved Mn^{2+} and Fe, however, rarely exceed 2 and 10 µM, respectively. Although it is clear that the Ba-bearing minerals in the sediments are different (e.g., $BaSO_4$) and more readily release Ba^{2+} than those hosting Mn and Fe, the order of magnitude lower dissolved concentrations of the latter are more likely attributable to solubility controls by metal sulfides. Evidence in support of this inference is available, particularly at Site 1006, where common pyrite in the sediments exemplifies the many orders of magnitude lower solubility product of this compound compared to that of Mn sulfide. This is reflected by a near absence of dissolved interstitial Fe^{2+} even where abundant source material is present.

CONCLUSIONS

Examination of results of minor and trace element determinations conducted aboard the *JOIDES Resolution* and in our laboratory reveal that extreme care should be taken when analyzing Li^+ onboard ship in the presence of extreme concentrations (mM range) of dissolved Sr^{2+}. Shipboard determinations of dissolved Sr^{2+} are extremely reliable. Results of shipboard determinations of dissolved Fe, however, are subject to artifacts including contamination and matrix effects. The passage of Fe colloids through 0.45-µm acrodiscs also leads to overestimation of the dissolved Fe content of interstitial water. Thus, filtration through 0.2-µm membranes is recommended if a more restricted measure of the dissolved Fe concentration is desired.

The minor and trace metal composition of pore fluids in sediments of the GBB transect sites is mediated principally by the effects on pore water properties of early diagenesis of carbonates resulting from the microbial degradation of organic matter, and by the abundance of detrital materials that serve as a source of these elements. Concentrations of dissolved Li^+ derive from two principal sources: (1) release from biogenic carbonate during their recrystallization, and (2) release from Li-bearing detrital phases by ion-exchange reactions with NH_4^+. The source of dissolved Sr^{2+} is almost exclusively biogenic carbonate, particularly aragonite. Concentrations of dissolved Sr^{2+}, however, are mediated by the presence of SO_4^{2-}, as are those of dissolved Ba^{2+}. The sources of the latter are primarily barite associated with remineralization of organic matter and, to a lesser extent, detrital minerals. Concentrations of Fe and Mn^{2+} in anoxic pore fluids are mediated by the insolubility of sulfides and incorporation into mixed carbonate minerals. The principal sources of these elements are easily reduced Fe-Mn-rich phases including Fe-rich clays found in lateritic soils and aeolian dust.

ACKNOWLEDGMENTS

We would like to acknowledge the Captain and crew of the *JOIDES Resolution* and the ODP technical staff for a very successful cruise. The able laboratory assistance of chemistry wizards Tim Bronk and Anne Pimmel was particularly helpful. Their dedication contributed greatly to the success of the shipboard inorganic geochemistry program. Technical assistance was provided at the SOEST atomic spectroscopy facilities by Charles M. Fraley and Ron Pflaum. FIA analyses were carried out by Cecily Chun and Toshiko Sato. Thoughtful critical reviews by H. J. Brumsack and R. W. Murray helped to considerably improve this paper. This research was funded in part by a postcruise research grant from JOI/USSP to EDC. This is SOEST contribution 5027.

REFERENCES

Baker, P.A., 1986. Pore-water chemistry of carbonate-rich sediments, Lord Howe Rise, Southwest Pacific Ocean. *In* Kennett, J.P., von der Borch, C.C., et al., *Init. Repts. DSDP,* 90: Washington (U.S. Govt. Printing Office), 1249–1256.

Baker, P.A., and Bloomer, S.H., 1988. The origin of celestite in deep-sea carbonate sediments. *Geochim. Cosmochim. Acta,* 52:335–339.

Baker, P.A., Gieskes, J.M., and Elderfield, H., 1982. Diagenesis of carbonates in deep-sea sediments: evidence from Sr^{2+}/Ca^{2+} ratios and interstitial dissolved Sr^{2+} data. *J. Sediment. Petrol.,* 52:71–82.

Ball, M.M., Martin, R.G., Bock, W.D., Sylvester, R.E., Bowles, R.M., Taylor, D.E., Coward, L. Dodd, J.E., and Gilbert, L., 1985. Seismic structure and stratigraphy of northern edge of Bahamian-Cuban collision zone. *AAPG Bull.*, 69:1275–1294.

Bischoff, J.L., Greer, R.E., and Luistro, A.O., 1970. Composition of interstitial waters of marine sediments: temperature of squeezing effect. *Science,* 167:1245–1246.

Bishop, J.K.B., 1988. The barite-opal organic carbon association in oceanic particulate matter. *Nature,* 332:341–343.

Bonatti, E., Fisher, D.E., Joensuu, O., Rydell, H., and Beyth, M., 1972. Iron-manganese-barium deposit from the northern Afar Rift (Ethiopia). *Econ. Geol.,* 67:717–730.

Boström, K., and Backman, J., 1990. Geochemistry and origin of Neogene sediments in Hole 711A. *In* Duncan, R.A., Backman, J., Peterson, L.C., et al., *Proc. ODP, Sci. Results,* 115: College Station, TX (Ocean Drilling Program), 699–708.

Bruland, K.W., 1983. Trace elements in seawater. *In* Riley, J.P., and Chester, R. (Eds.), *Chemical Oceanography* (Vol. 8): London (Academic Press), 157–220.

Claypool, G.E., and Kaplan, I.R., 1974. The origin and distribution of methane in marine sediments. *In* Kaplan, I.R. (Ed.), *Natural Gases in Marine Sediments:* New York (Plenum), 99–139.

De Carlo, E.H., 1992. Geochemistry of pore water and sediments recovered from the Exmouth Plateau. *In* von Rad, U., Haq, B.U., et al., *Proc. ODP, Sci. Results,* 122: College Station, TX (Ocean Drilling Program), 295–308.

Dehairs, F., Chesselet, R., and Jedwab, J., 1980. Discrete suspended particles of barite and the barium cycle in the open ocean. *Earth Planet. Sci. Lett.,* 49:528–550.

Dehairs, F., Lambert, C.E., Chesselet, R., and Risler, N., 1987. The biological production of marine and suspended barite and the barium cycle in the Western Mediterranean Sea. *Biogeochemistry,* 4:119–139.

Denny, W.M., Austin, J.A., and Buffler, R.T., 1994. Seismic stratigraphy and geologic history of mid-Cretaceous through Cenozoic rocks, Southern Straits of Florida. *AAPG Bull.,* 87:461–487.

Duce, R.A., Liss, P.S., Merrill, J.T., Atlas, L.L., Buat-Menard, P., Hicks, B.B., Miller, J.M., Prospero, J.M., Arimoto, R., Church, T.M., Ellis, W., Galloway, J.N., Hansen, L., Jickells, T.D., Knap, A.H., Reinhardt, K.H., Schneider, B., Soudine, A., Tokos, J.J., Tsunogai, S., Wollast, R., and Zhou, M., 1991. The atmospheric input of trace species to the world ocean. *Global Biogeochem. Cycles,* 5:193–259.

Eberli, G.P., Swart, P.K., Malone, M.J., et al., 1997. *Proc. ODP, Init. Repts.,* 166: College Station, TX (Ocean Drilling Program).

Francois, R., Honjo, S., Manganini, S.J., and Ravizza, G.E., 1995. Biogenic barium fluxes to the deep sea: implications for paleoproductivity reconstruction. *Global Biogeochem. Cycles,* 9:289–303.

Froelich, P.N., Mortlock, R.A., Mefferd, M., and Powers, J., 1991. Interstitial-water chemistry: abyssal South Atlantic and East Georgia Basins, Islas Orcadas and Meteor Rises. *In* Ciesielski, P.F., Kristoffersen, Y., et al., *Proc. ODP, Sci. Results,* 114: College Station, TX (Ocean Drilling Program), 719–731.

Gieskes, J.M., 1981. Deep-sea drilling interstitial water studies: implications for chemical alteration of the oceanic crust, layers I and II. *In* Warme, J.E., Douglas, R.G., and Winterer, E.L. (Eds.), *The Deep Sea Drilling Project: A Decade of Progress.* Spec. Publ.—Soc. Econ. Paleontol. Mineral., 32:149–167.

————, 1983. The chemistry of interstitial waters of deep-sea sediments: interpretation of deep-sea drilling data. *In* Riley, J.P., and Chester, R. (Eds.), *Chemical Oceanography* (Vol. 8): London (Academic), 221–269.

Heinrichs, H., and Herrmann, A.G., 1990. *Praktikum der Anatytischen Geochemie:* Berlin (Springer Verlag).

Hoefs, J., and Sywall, M., 1997. Lithium isotope composition of Quaternary and Tertiary biogene carbonates and a global lithium isotope balance. *Geochim. Cosmochim. Acta*, 61:2679–2690.

Kabata-Pendias, A., and Pendias, H., 1992. *Trace Elements in Soils and Plants:* Boca Raton, FL (CRC Press).

Mottl, M.J., 1992. Pore waters from serpentinite seamounts in the Mariana and Izu-Bonin forearcs, Leg 125: evidence for volatiles from the subducting slab. *In* Fryer, P., Pearce, J.A., Stokking, L.B., et al., *Proc. ODP, Sci. Results,* 125: College Station, TX (Ocean Drilling Program), 373–385.

Mottl, M.J., and Holland, H.D., 1978. Chemical exchange during hydrothermal alteration of basalt by seawater, I. Experimental results for major and minor components of seawater. *Geochim. Cosmochim. Acta,* 42:1103–1115.

Mullins, H.T., and Lynts, G.W., 1977. Origin of the north-western Bahama Platform: review and reinterpretation. *Geol. Soc. Am. Bull.*, 88:1447–1461.

Paytan, A., 1995. Marine barite, a recorder of oceanic chemistry, productivity, and circulation [Ph.D. thesis]. Scripps Inst. Oceanogr., Univ. Calif. San Diego.

Prospero, J.M., 1996. Saharan dust transport over the North Atlantic Ocean and Mediterranean: an overview. *In* Guerzoni, S., and Chester, R. (Eds.), *The Impact of African Dust Across the Mediterranean:* Dordrecht (Kluwer), 133–152.

Resing, J.A., and Mottl, M.J., 1992. Determination of manganese in seawater using flow injection analysis with on-line preconcentration and spectrophotometric detection. *Anal. Chem.,* 64:2682–2687.

Robinson, J.W., 1990. *Atomic Spectroscopy:* New York (Marcel Dekker).

Schmitz, B., 1987. Barium, equatorial high productivity, and the northward wandering of the Indian continent. *Paleoceanography,* 2:63–77.

Schroeder, J.O., Murray, R.W., Leinen, J., Pflaum, R.C., and Janecek, T.R. 1997. Barium in equatorial Pacific carbonate sediment: terrigenous, oxide, and biogenic associations. *Paleoceanography*, 12:125–146.

Sheridan, R.E., Corsby, J.T., Bryan, G.M., and Stoffa, P.L., 1981. Strratigraphy and structure of southern Blake Plateau, Northern Florida Straits, and Northern Bahama Platform from multichannel seismic reflection data. *AAPG Bull.*, 65:2571–2593.

Shipboard Scientific Party, 1997a. Leg synthesis: sea-level changes and fluid flow on the Great Bahama Bank slope. *In* Eberli, G.P., Swart, P.K., Malone, M.J., et al., *Proc. ODP, Init. Repts.,* 166: College Station, TX (Ocean Drilling Program), 13–22.

Shipboard Scientific Party, 1997b. Site 1005. *In* Eberli, G.P., Swart, P.K., Malone, M.J., et al., *Proc. ODP, Init. Repts.,* 166: College Station, TX (Ocean Drilling Program),

Sigurdsson, H., Leckie, R.M., Acton, G.D., et al., 1997. *Proc. ODP, Init. Repts.,* 165: College Station, TX (Ocean Drilling Program).

von Breymann, M.T., Brumsack, H., and Emeis, K.C., 1992. Depositional and diagenetic behavior of barium in the Japan Sea. *In* Pisciotto, K.A., Ingle, J.C., Jr., von Breymann, M.T., Barron, J., et al., *Proc. ODP, Sci. Results,* 127/128 (Pt. 1): College Station, TX (Ocean Drilling Program), 651–665.

Walles, F., 1993. Tectonic and diagenetically induced seal failure with the south-western Great Bahamas Bank, Caprocks. *Mar. Pet. Geol.*, 10:14–28.

Date of initial receipt: 18 August 1998
Date of acceptance: 8 February 1999
Ms 166SR-118